Shubnikov–de Haas Measurements in $Pb_{1-x}Sn_xTe$*

John Melngailis, T. C. Harman, J. G. Mavroides, and J. O. Dimmock
Lincoln Laboratory, Massachusetts Institute of Technology, Lexington, Massachusetts 02173
(Received 10 August 1970)

Oscillatory-magnetoresistance measurements have been carried out on various samples of $Pb_{1-x}Sn_xTe$. Compositions ranged from $x=0.16$ to $x=0.32$, carrier concentrations from 3×10^{16} to 1.8×10^{18}, and most of the samples were p type. The Fermi surface was found to consist of prolate ellipsoids oriented along the [111] axis at the L points. The ellipsoid-anisotropy ratio K has values between 10.5 and 11.2, and within an accuracy of about 10% is independent of carrier concentration and of x within the above range. Effective masses and g factors were also determined. For example, a sample with $x=0.216$ and with a hole density of 8.5×10^{17} cm^{-3} was found to have a transverse mass $m^*_{111}=0.0225m$, where m is the free electron mass. The mass was observed to decrease with decreasing carrier density. Clear spin splitting was observed in the [110] and [100] directions in this sample with $g_{110}=52$ and $g_{100}=37$. The ratio of spin splitting to Landau-level spacing was found to be approximately 0.68 for both directions. The carrier density as determined by Hall measurements agrees with the number of states calculated from the measured Fermi-surface dimensions. Extra frequency branches such as those observed by Burke *et al.* in SnTe and in $Pb_{0.87}Sn_{0.13}Te$ were not found.

INTRODUCTION

The semiconductor $Pb_{1-x}Sn_xTe$ has the NaCl crystal structure with an energy gap dependent on composition x. For low tin-telluride concentrations, the gap decreases with increasing x and is believed to pass through zero at an intermediate composition and to increase with x for high SnTe concentrations. Although there is an inherent disorder of the Pb-Sn atoms of the metal sublattice of the alloy single crystals, the carrier mobilities remain high and are only slightly reduced from those of PbTe. As a result of the relatively high degree of crystalline perfection, infrared lasers[1] and detectors[2] operating over a wide range of wavelengths have been made from $Pb_{1-x}Sn_xTe$.

$Pb_{1-x}Sn_xTe$ is generally doped by slight departures from stoichiometry, i.e., an excess of metal yields n-type material, whereas an excess of Te yields p type. These excess carriers do not freeze out at helium temperatures. Thus, a study of the Fermi-surface geometry and the band parameters at the Fermi level is possible.[3–6] In this paper, we report on Shubnikov–de Haas measurements made primarily on p-type $Pb_{1-x}Sn_xTe$ samples with $0.16<x<0.32$. First, the experimental techniques, then the results, and finally the theoretical understanding of the results are discussed.

EXPERIMENTAL

The growth and preparation of samples has been described previously.[2,4] Briefly, 4×12-mm wafers were cut from Bridgeman-grown single-crystal ingots and etch polished to a thickness of 0.25 mm. The large area surfaces were {100} or {110} planes. The specimens were then annealed in appropriate atmospheres for periods up to 60 days at temperatures between 650 and 400 °C to produce homogeneous samples of the desired carrier concentrations. Oriented samples of typical dimensions $2\times0.7\times0.25$ mm were cut from the wafers with a wire saw. The long axis was cut parallel to the [110] direction. The samples were then etched electrolytically.[2,7] Contacts were usually made with liquid solder and occasionally by electroplating gold followed by electroplating indium.[4]

The samples were mounted with the long dimension vertical. The magnetic field produced by either a 12-in. Varian or a Helmholtz coil 90-kG Bitter magnet was in the horizontal plane. The temperature was measured to better than ±0.03 °K by a Macleod gauge and by a calibrated Ge resistance thermometer mounted near the sample directly in the liquid helium.

The derivative of the transverse magnetoresistance vs magnetic field was measured by the standard technique. The magnetic field was modulated at 40 Hz with an amplitude of 100 G peak to peak, maintained constant by a servo system. While the current through the sample was maintained constant at say, 30 mA, the voltage across the sample was fed to a phase-sensitive lock-in amplifier (P.A.R. HR-8) detecting at the modulation frequency. The output of the lock-in drove the y axis of a x-y recorder. The x axis was driven proportional to the magnetic field by the output of a linear Hall probe.

BACKGROUND AND ANALYSIS

For the low magnetic fields and for spherical Fermi surfaces, theoretical expressions have been derived for the transverse oscillatory magnetoresistance,[8,9]

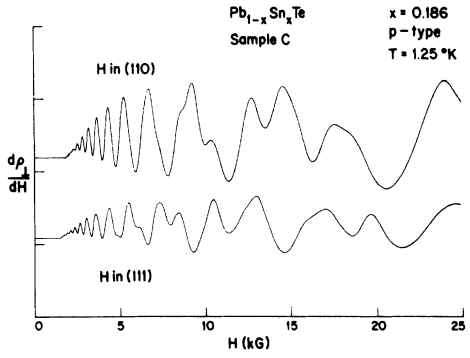

FIG. 1. Recorder trace plotting the derivative of the transverse magnetoresistance as a function of magnetic field for sample C.

$$\rho_\perp = \rho_0\left[1+\frac{5}{2}\sum_{r=1}^{\infty} b_r \cos\left(\frac{2\pi r E_F}{\hbar\omega_c}-\tfrac{1}{4}\pi\right)+R\right], \tag{1}$$

with

$$b_r = \frac{(-1)^r}{r^{1/2}}\left(\frac{\hbar\omega_c}{E_F}\right)^{1/2}\frac{2\pi^2 r kT/\hbar\omega_c}{\sinh(2\pi^2 r kT/\hbar\omega_c)}$$

$$\times\cos(\pi r\nu)e^{-2\pi^2 kT_D/\hbar\omega_c}.$$

The symbols have their usual meanings. E_F is the Fermi energy, ω_c is the cyclotron frequency, ν is the ratio of spin splitting to Landau-level spacing, and T_D is the Dingle temperature, representing the effect of collision broadening. The quantity R represents an additional series of oscillating terms which is generally much smaller than the term shown. This result has been extended to general dispersion relations.[10] A similar expression holds except that the oscillatory term $(-1)^r \times\cos(2\pi r E_F/\hbar\omega_c-\frac{1}{4}\pi)$, becomes $\cos(2\pi r\alpha/H-2\pi r\gamma-\frac{1}{4}\pi)$; γ is a phase ($\gamma=\frac{1}{2}$ for parabolic bands). The frequency α is given by

$$\alpha=(\hbar c/2\pi e)A, \tag{2}$$

where A is an extremal Fermi-surface cross-sectional area perpendicular to the magnetic field. The cyclotron frequency $\omega_c=eH/m^*c$ is defined through the expression for the cyclotron effective mass

$$m^*=\frac{\hbar^2}{2\pi}\frac{\partial A}{\partial E_F}. \tag{3}$$

From the period of the oscillations in Figs. 1 and 2, the extremal areas of the Fermi surface are obtained using Eq. (2). The effective mass is deduced from the temperature dependence of the amplitude of the sinusoidal oscillations while the g factor is gotten from the spin splitting, which is clearly observed at the higher magnetic fields in Fig. 2.

We have taken the values thus determined, inserted them in Eq. (1) and computed $d\rho_\perp/_{dH}$ vs H. The resulting curve closely resembles that in Fig. 1, except above about 10 kG the amplitude envelope of the experimental curve grows much more slowly than the envelope of the calculated curve. This is believed to be due to the fact that the assumption $\hbar\omega_c \ll E_F$, made in deriving Eq. (1), is no longer valid. The experimentally observed spin splitting at low magnetic fields appears to be the same as that calculated by Eq. (1).

To extract some of the higher-frequency components from the experimental curves we have used a computer filtering technique.[11] The experimental trace is first digitized using a Calma model No. 485 digitizer. In this form the trace is made the driving term of a linear differential equation describing, for example, a series resonant circuit

$$\frac{d^2y}{dx^2}+\beta\frac{dy}{dx}+4\pi^2 f^2 y=F(x), \tag{4}$$

where

$$x=\frac{1}{H}\quad\text{and}\quad F(x)=\frac{d\rho_\perp(H)}{dH}\bigg|_{H=1/x}.$$

The equation is solved for different values of its resonant frequency f, and the response $\int y^2\,dx$ is plotted as a function of f as in Fig. 3. Peaks are observed at the various frequencies that make up the trace $F(x)$. For the sake of comparison, Burke has analyzed two of our traces by the Fourier technique.[3,12,13] Although the detailed shape of the frequency spectrum curve is somewhat different from Fig. 3, the peaks appear in the same positions, i.e., no additional frequencies were

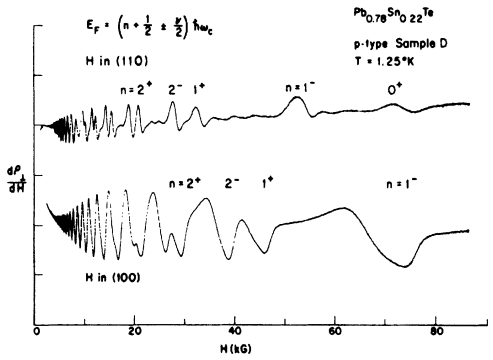

FIG. 2. Same plot as Fig. 1 for sample D extended to high fields. The upper (110) trace is taken with the modulating field perpendicular to the applied field. This suppressed the higher-frequency oscillations, which are barely visible between the $n=2$ and $n=0$ peaks. The lower 100 trace as well as those in Fig. 1 are taken with the usual technique with the modulating field parallel to the applied field.

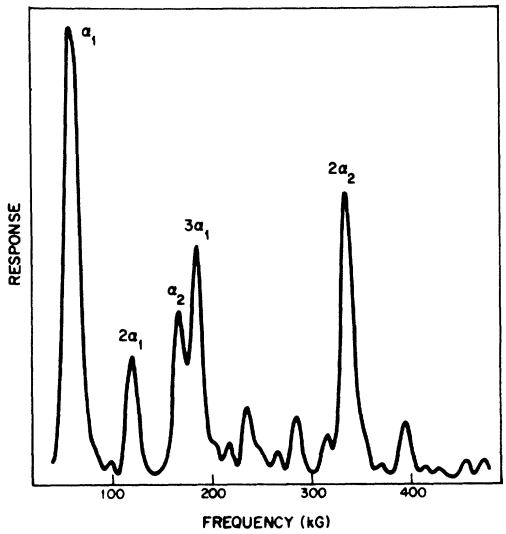

FIG. 3. Frequency analysis of the (110) experimental trace, for sample D (up to 25 kG) showing harmonics of the main frequency α_1 at 60 kG, its harmonics, and the frequency due to the maximum cross section α_2 at 167 kG. The large peak at 335 kG is the second harmonic of this indicating that the spin-splitting factor ν is nearly equal to 0.5. This second-harmonic frequency is in fact the one barely visible between the spin-split peaks in Fig. 2.

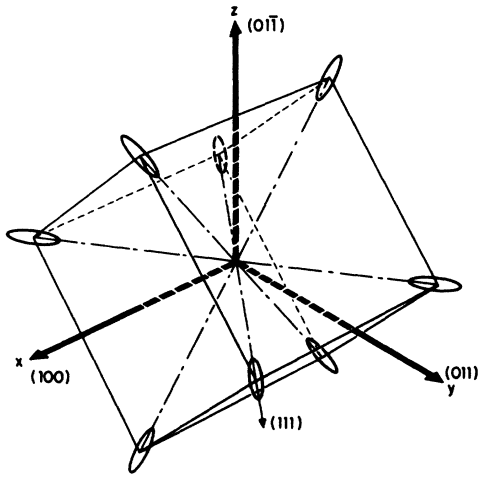

FIG. 4. Schematic of the Fermi surface (pockets of either holes or electrons in k space) for the lead salts in the orientation used in our measurements. The direction of the magnetic field was varied in the x-y plane, while the current was flowing in the z direction. The cube standing on edge is not the Brillouin zone, but merely an aid to visualization.

observed similar to those reported earlier.[3,13]

RESULTS

By measuring the oscillatory magnetoresistance for p-type samples as a function of magnetic field for various directions of the field in the (110) plane, we find that the Fermi surface in the alloys, as in PbTe, consists of prolate ellipsoids lying along the [111] axis at the L points in the Brillouin zone (Fig. 4). The frequencies (areas) for sample D are plotted in Fig. 5 as a function of angle from the long axis of the ellipsoids. The plot indicates that the Fermi surface is ellipsoidal within experimental error, with an anisotropy ratio $K = 11.2 \pm 0.5$. (K is defined as the square of the ratio of maximum cross-sectional area to the minimum area.) This value agrees with other work.[3] We find also that, as seen in Table I, K does not change significantly for samples with x between 0.18 and 0.30 and with 2×10^{17}–2×10^{18} holes/cm^3. The transverse effective mass m^*_{111}, however, does change with carrier concentration and with SnTe content x. The values found agree with those of Ref. 3, where a comparison can be made. For the n-type sample, the Fermi-surface areas larger than the (100) area could not be measured. However, up to that point the shape of the electron surfaces seems to be the same as that of the hole surfaces.

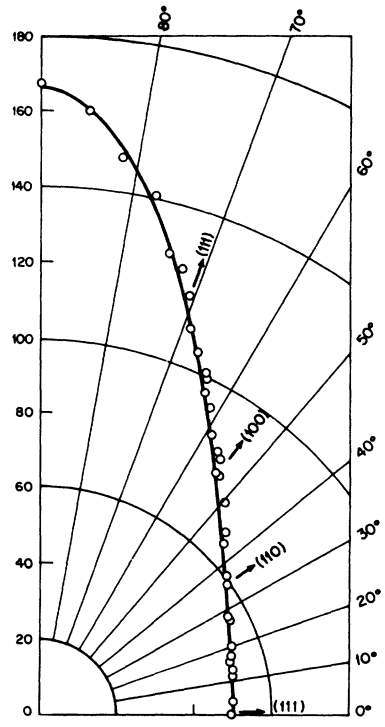

FIG. 5. Polar plot of the Shubnikov–de Haas frequencies for sample D. The solid line is a calculated ellipse with ratio of axis $\sqrt{11.2}$. The frequencies α are in kG. The conversion to actual area in reciprocal space is given by $A = 0.956\times10^8$ G^{-1} cm$^{-2}\times\alpha$.

TABLE I. Properties of $Pb_{1-x}Sn_xTe$ at 4.2 °K.

Sample	x	Type	Carrier conc	K	A_{111} (10^{12} cm^{-2})	m^*_{111}/m	m^*_{111}/m (two band)	Calc (six band)
Ref. 14	0	n	band edge	10 ± 1.5		0.024 ± 0.003	0.023	0.023
A	0.164 ± 0.005	n	4.3×10^{16}		0.746	0.014 ± 0.002	0.0139	0.0150
Ref. 15	0	n	2.15×10^{18}	11				
Ref. 14	0	p	band edge	14 ± 2		0.022 ± 0.003	0.023	0.023
Ref. 15	0	p	2.14×10^{17}	13				
Ref. 12	0	p	3×10^{18}	13	10.5	0.036 ± 0.002	0.0339	0.0332
Ref. 3	0.13	p	4.5×10^{17}	12.0		0.0197		
Ref. 3	0.19	p	4.3×10^{17}			0.0195		
Ref. 3	0.30	p	1.3×10^{18}	11.0		0.0257		
B	0.185 ± 0.005	p	3.1×10^{16}		0.642	0.0120 ± 0.0015	0.0125	0.0136
C	0.186	p	2.6×10^{17}	10.5 ± 1.0	2.14	0.0160 ± 0.0015	0.0155	0.0167
D	0.216	p	8.5×10^{17}	11.2 ± 0.5	4.78	0.0225 ± 0.0015	0.0189	0.0202
E	0.310	p	2.2×10^{17}	10.5 ± 1.0	1.89	0.0140 ± 0.0015	0.0108	0.0119
F	0.315	p	1.8×10^{18}	10.5 ± 0.7	7 30	0.0275 ± 0.002	0.0208	0.0225

In the Shubnikov–de Haas work on SnTe [13] and $Pb_{1-x}Sn_xTe$,[3] extra frequency branches have been observed. These frequencies all have similar angular dependence.[3,13] We do not see such extra frequencies. For example, in the (100) trace in Fig. 2 there is only one frequency visibly present until the spin splitting becomes prominent. The frequency analysis also reveals no extra branches. [The two extra peaks at 285 and 395 kG, in Fig. 3, although they appear in one other (110) run, do not appear at other angles. We have no explanation for them but feel they do not represent extra frequency branches of the type observed in Ref. 3.]

From the splitting of the oscillations at high magnetic field, Fig. 2, we obtain the quantity $\nu = gm^*/2m_0$ in the manner shown in Fig. 6. We plot the positions at which the derivative $d\rho_L/dH$ crosses zero as a function of quantum number. These are the positions at which the Landau levels of given quantum number and spin pass through the Fermi level. The ratio of the spin splitting in $1/H$ to the period $\Delta(1/H)$ is then ν. The values of ν for $Pb_{1-x}Sn_xTe$ are seen in Table II to be larger than in PbTe. As in PbTe [12] the number of states in the [111] ellipsoids, Fig. 4, as calculated from the measured Fermi-surface dimensions agrees with the number of carriers deduced from high-field Hall measurements within 10%. Because of the small dimensions of the samples used, the uncertainty in the Hall constant R_H is at least 10%. The carrier concentration was assumed given by $1/R_He$.

DISCUSSION

The $k\cdot p$ model for the valence and conduction bands in PbTe has been extended to $Pb_{1-x}Sn_xTe$.[19] In this theory, six parameters in the dispersion relation were chosen to fit known band-edge properties of PbTe, and then the energy gap E_g was taken as the only variable parameter across the alloy system.

The general dispersion relation in this model is[12,19]

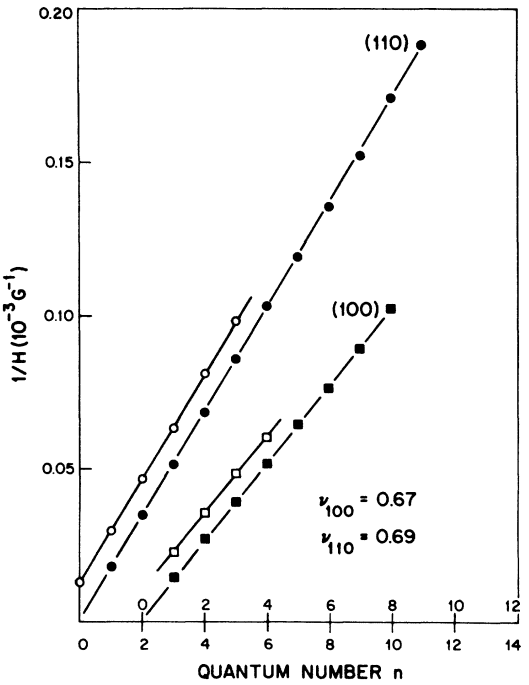

FIG. 6. Reciprocals of the values of magnetic field at which the traces in Fig. 2 cross zero (average) are plotted against the corresponding quantum numbers. The upper scale of n refers to the (100) points, the lower to the (110). The slope is the Shubnikov–de Haas period $\Delta(1/H)$ while the vertical difference between the open and solid points for each n is the spin splitting Δ_s. Then $\nu = \Delta_s/\Delta(1/H)$. The intersection of the line drawn midway between the spin-split points and the vertical axis ($n = 0$) occurs close to $\frac{1}{2}\Delta(1/H)$. This is expected since the positions of the points is given by $1/H_n = (n + \frac{1}{2} \pm \frac{1}{2}\nu)\Delta(1/H)$.

TABLE II. Effective g factors in $Pb_{1-x}Sn_xTe$ (corresponding values of ν shown in parenthesis).

Reference	x	Type and carrier conc	$g_{\parallel}(\nu_{\parallel})$	$g_{\perp}(\nu_{\perp})$	$g_{110}(\nu_{110})$	$g_{100}(\nu_{100})$
16	0	$n=8-\times10^{16}$	57.5 ± 2	15 ± 1	46	35.5
15	0	$n=1.5\times10^{18}$	(0.57 ± 0.02)			
17	0	p-n junction				29[a]
14	0	$n=0$	45 ± 8			
14	0	$p=0$	51 ± 8			
12	0	$p=3\times10^{18}$	32 ± 2 (0.58)	7 ± 2 (0.27)		23 ± 5 (0.58)
18	0.19	p-n junction				77[a]
18	0.21	p-n junction				84[a]
18	0.26	p-n junction				112[a]
18	0.27	p-n junction				130[a]
This work sample D	0.216±0.005	$p=0.85\times10^{18}$		(0.50)	52 ± 4 (0.69)	37 ± 3 (0.67)

[a] The assumption is made that $g_{\text{conduction}}=g_{\text{valence}}$.

$$\left(E-\tfrac{1}{2}E_g-\frac{\hbar^2}{2m_t^-}(k_x^2+k_y^2)-\frac{\hbar^2}{2m_l^-}k_z^2\right)\times\left(E+\tfrac{1}{2}E_g+\frac{\hbar^2}{2m_t^+}(k_x^2+k_y^2)+\frac{\hbar^2}{2m_l^+}k_z^2\right)=\frac{\hbar^2}{m^2}[P_\perp^2(k_x^2+k_y^2)+P_\parallel^2k_z^2], \tag{5}$$

where $P_\parallel$ and $P_\perp$ represent the interaction of the valence and conduction bands, and $m_t^\pm$ and $m_l^\pm$ represent the effect of the more distant bands. The transverse effective mass m_{111}^* can be derived by setting $k_z=0$ and using Eq. (3). In PbTe, m_{111}^* is the same for holes and electrons within experimental accuracy.[14] This would imply that $m_t^+=m_t^-$. With this assumption, the expression for m_{111}^* is

$$\frac{m_{111}^*}{m}=\frac{\{[\tfrac{1}{2}E_g+(m/m_t^+)A']^2+E_\perp A'\}^{1/2}}{[\tfrac{1}{2}E_g+(m/m_t^+)A'](m/m_t^+)+\tfrac{1}{2}E_\perp}, \tag{6}$$

where $E_\perp=2P_\perp^2/m$ and $A'=\hbar^2A/2\pi m$. Using the expression for the gap as a function of composition,[20] $E_g=0.19$ eV $[(1-x)/0.35]$, taking $E_\perp=6.73$ eV and $m/m_t^+=8.1$, the values of m_{111}^*/m shown in the last column in Table I are calculated. This choice of $E_\perp$ and m/m_t^+ gave the best over-all fit. The fact that there remains a consistent difference between the calculated and measured values indicates that contrary to what is assumed in the model, perhaps $E_\perp$ and m/m_t^+ vary across the alloy system. The two-band model with $E_\perp=8.26$ eV and $m/m_t^+=0$ is seen in Table I to give a somewhat poorer fit. Using the values of the parameters given in Ref. 19 gives a fit intermediate between the two.

The lack of significant variation of the ellipsoid anisotropy K with carrier concentration agrees qualitatively with the model and the parameters given in Ref. 19. However, K in Table I seems to decrease in going from PbTe $x=0$ to the alloys with $x=0.18$–0.30, while this model predicts about a 10% increase for $x=0.21$.

The behavior of the spin splitting, Table II, qualitatively agrees with the theory. As x increases and the gap decreases, ν approaches closer to 1. The smaller the direct gap, the closer one is to the case described by the two-band model, which predicts $\nu=1$.

In Fig. 2, the $n=1^-$ quantum oscillation for the (100) trace gives some indication about the actual shape of the magnetoresistance peak. It rises slowly from 50 to 65 kG, then decreases more rapidly from 65 to 75 kG, and finally the derivative goes to its average value rather abruptly at 75–80 kG, indicating that $\rho(H)$ has a corner. This shape is qualitatively in agreement with the type of broadening of the density-of-states peaks discussed in Ref. 9, Figs. 4 and 6.

In general, the Fermi surface of $Pb_{1-x}Sn_xTe$, up to the band crossing point, has the same shape as that of PbTe, except that the anisotropy factor K is somewhat smaller, the spin splitting is larger, and the effective mass is smaller.

ACKNOWLEDGMENTS

We wish to thank the following members of our laboratories for their help: Mary C. Finn for electron microprobe analysis, Ivars Melngailis and S. H. Groves for useful discussions, W. C. Kernan for highly competent technical assistance, N. B. Childs for assistance with curve digitizing, Susan N. Landon and Nancy S. Brine for advice on computer programming, E. L. Mastromattei for sample x-ray orientation, Katherine M. Nearen for sample cutting, Mary L. Barney for advice on etching and contacts, and A. E. Paladino and J. H. Boghos for crystal growing and annealing. We are grateful to J. R. Burke for sending us his results prior to publication.

†Work sponsored by the Department of the Air Force.
*Part of this work was performed at the Francis Bitter National Magnet Laboratory, M.I.T.

[1]A review of narrow-gap semiconductor infrared lasers is given by T. C. Harman, in Proceedings of the Conference on the Physics of Semimetals and Narrow Gap Semiconductors, Dallas, 1970 (unpublished); J. Phys. Chem. Solids Suppl. (to be published).

[2]A review of the lead-tin chalcogenides, their preparation, properties, and applications as detectors is given by Ivars Melngailis and T. C. Harman, in *Semiconductors and Semimetals*, edited by R. K. Willardson and A. C. Beer (Academic, New York, 1970), Vol. VII.

[3]J. R. Burke, J. D. Jensen, and B. Houston, Ref. 1.

[4]John Melngailis, J. A. Kafalas, and T. C. Harman, Ref. 1.

[5]G. A. Antcliffe, R. T. Bate, and J. S. Wrobel, Bull. Am. Phys. Soc. 14, 330 (1969).

[6]John Melngailis, T. C. Harman, J. G. Mavroides, and J. O. Dimmock, Bull. Am. Phys. Soc. 14, 330 (1969).

[7]M. K. Norr, J. Electrochem. Soc. 109, 433 (1962).

[8]L. A. Roth and P. N. Argyres, in *Semiconductors and Semimetals*, edited by R. K. Willardson and A. C. Beer (Academic, New York, 1966), Vol. I, p. 185.

[9]R. Kubo, S. J. Miyake, and N. Hashitsume, in *Solid State Physics*, edited by F. Seitz and D. Turnbull (Academic, New York, 1965), Vol. 17, p. 361; A. H. Kahn and H. P. R. Fredrikse, *ibid.*, Vol. 9.

[10]I. M. Lifshitz and A. M. Kosevich, Zh. Eksperim. i Teor. Fiz. 29, 730 (1955) [Soviet Phys. JETP 2, 636 (1956)]; J. Phys. Chem. Solids 4, 1 (1958).

[11]P. T. Panousis, Ph.D. thesis, Iowa State University, 1967 (unpublished). The main subroutines and instruction on their use were kindly provided by H. A. Ashworth of Carnegie-Mellon University.

[12]J. R. Burke, B. Houston, and H. T. Savage, Phys. Rev. B 2, 1977 (1970).

[13]J. R. Burke, B. Houston, H. T. Savage, J. Babiskin, and P. G. Liebermann, J. Phys. Soc. (Dunod, Paris, 1964), 384 (1966).

[14]K. F. Cuff, M. R. Ellett, C. D. Kuglin, and L. R. Williams, in *Proceedings of International Conference on the Physics of Semiconductors* (Dunod, Paris, 1964), p. 677.

[15]W. Schilz, J. Phys. Chem. Solids 30, 893 (1969).

[16]C. K. N. Patel and R. E. Slusher, Phys. Rev. 177, 1200 (1969).

[17]J. F. Butler and A. R. Calawa, in *Physics of Quantum Electronics*, edited by P. L. Kelley, B. Lax, and P. E. Tannenwald (McGraw-Hill, New York, 1966), pp. 458–466.

[18]J. F. Butler, Solid State Commun. 7, 909 (1969).

[19]J. O. Dimmock, Ref. 1.

[20]J. F. Butler and T. C. Harman, IEEE J. Quantum Electron. QE5, 50 (1969); Ivars Melngailis and A. R. Calawa, Appl. Phys. Letters 9, 304 (1966).

PHYSICAL REVIEW B VOLUME 3, NUMBER 2 15 JANUARY 1971

Infrared Absorption in *p*-Type GaP

J. D. Wiley and M. DiDomenico, Jr.
Bell Telephone Laboratories, Murray Hill, New Jersey 07974
(Received 1 September 1970)

Infrared absorption measurements have been performed on Zn-doped GaP at 300 and 90 °K. The absorption observed at 300 °K between 1 and 12 μ is attributed to a combination of intraband free-carrier absorption (FCA) and direct interband absorption arising from transitions between the Γ_8 and Γ_7 (splitoff) valence bands. The absorption at 90 °K is identified as photoionization of holes from the Zn acceptor levels to the Γ_8 and Γ_7 valence bands. Because of the small spin-orbit splitting (82 meV) and strong nonparabolicity of the valence bands in GaP, both the interband and intraband absorption are qualitatively different from similar absorption in other III-V compounds. The interband transitions give rise to extremely broad overlapping absorption bands while the FCA exhibits an unusually large magnitude. We propose a model for FCA in *p*-GaP which includes the effect of virtual intermediate states in the light-hole and splitoff valence bands. It is shown, on the basis of this model, that FCA in *p*-GaP should have a wavelength dependence which depends on the scattering mechanism in the usual way, but whose magnitude is enhanced by the additional intermediate states. In agreement with transport measurements, we find that holes are scattered principally by acoustic and nonpolar optical phonons.

I. INTRODUCTION

Infrared absorption has proved to be an extremely valuable tool in the study of energy band structures, lattice vibrations, and scattering mechanisms in semiconductors.[1] In the case of GaAs, for example, infrared absorption has yielded important information about the conduction[2–4] and valence-band structures,[5,6] lattice vibrational modes,[7,8] and the scattering mechanisms for free carriers.[9–11] Similar success has been obtained in infrared studies of the $GaAs_{1-x}P_x$ alloy system[12–15] and of *n*-type GaP.[16–20] The case of *p*-type GaP, however, is complicated by the unusually small spin-orbit split-